Potential Predictability of North China Summer Drought

LIXIA ZHANG

State Key Laboratory of Numerical Modeling for Atmospheric Sciences and Geophysical Fluid Dynamics, Institute of Atmospheric Physics, Chinese Academy of Sciences, Beijing, and Collaborative Innovation Center on Forecast and Evaluation of Meteorological Disasters, Nanjing University of Information Science and Technology, Nanjing, China

TIANJUN ZHOU

State Key Laboratory of Numerical Modeling for Atmospheric Sciences and Geophysical Fluid Dynamics, Institute of Atmospheric Physics, Chinese Academy of Sciences, Beijing, China

PEILI WU

Met Office Hadley Centre, Exeter, United Kingdom

XIAOLONG CHEN

State Key Laboratory of Numerical Modeling for Atmospheric Sciences and Geophysical Fluid Dynamics, Institute of Atmospheric Physics, Chinese Academy of Sciences, Beijing, China

(Manuscript received 11 October 2018, in final form 1 July 2019)

ABSTRACT

Any skillful prediction is of great benefit to North China, a region that is densely populated and greatly impacted by droughts. This paper reports potential predictability of North China summer drought 1 month ahead based on hindcasts for 1961–2005 from the "ENSEMBLES" project. Correlation scores of the standardized precipitation–evapotranspiration index and standardized precipitation index reach 0.49 and 0.39, respectively. The lower-level northwestern Pacific cyclonic circulation anomaly (NWPCCA) and East Asian upper-tropospheric temperature (UTT) cooling are the crucial circulations with regard to summer drought. Two sources of predictability are identified: 1) Pacific–Japan and Silk Road teleconnections forced by well-established eastern Pacific Ocean El Niño sea surface temperature anomalies (SSTA) in summer, when the two key circulations are both well predicted because of a good prediction of enhanced equatorial central Pacific (CP) rainfall and Indian rainfall deficit, and 2) the subtropical atmosphere–ocean coupling associated with CP El Niño developing, when the skill mainly arises from the reasonable prediction of NWPCCA. In observations, the NWPCCA persists from the preceding spring to summer through a wind–evaporation–SST feedback related to the Pacific meridional mode (PMM). In predictions, the persistence of the NWPCCA is mainly forced by the enhanced convection over the subtropical central North Pacific due to the persistence of the PMM-related meridional SSTA gradient over the CP. This predicted SSTA suppresses the equatorial Pacific rainfall, contributing to low prediction skill for the East Asian UTT cooling. This study demonstrates the importance of extratropical signals from the preceding season in North China summer drought prediction.

1. Introduction

As the most populous region in China and a major agricultural and industrial sector, North China has been hit by frequent severe droughts in the past that exerted severe economic and environmental impacts and worsened the local water crisis (Ma and Fu 2006; Zhou et al. 2009). Drought disasters over North China feature the widest coverage, highest intensity, and longest duration when compared with the other regions of China (Zhang and Zhou 2015; Yang et al. 2013). A reliable drought forecast of North China can provide a useful drought early warning and help local government to manage the drought risk and alleviate drought impacts. It is desirable to investigate the seasonal predictability of drought over North China and to understand the underlying mechanisms.

Dynamical forecasts based on coupled atmosphere–ocean–land general circulation models are a promising

Corresponding author: Lixia Zhang, lixiazhang@mail.iap.ac.cn

DOI: 10.1175/JCLI-D-18-0682.1

tool and have been increasingly used for drought prediction globally (Dutra et al. 2014; Mo and Lyon 2015). Given that meteorological drought is the main cause of agricultural failures and hydrological water shortages, predictions of precipitation and temperature are thus crucial for drought forecast and early warning. Hence, the prediction of meteorological drought represented by drought indices related to precipitation and temperature is examined in this study. Extensive analysis has shown that prediction skill of summer precipitation over China is relatively low (Wang et al. 2009; Kim et al. 2012; Kang et al. 2002; Luo et al. 2013), although the current seasonal forecast systems can predict the large-scale circulation anomalies, such as the leading interannual modes (Yang et al. 2008; Kim et al. 2012; Gao et al. 2015), and the variations of the key climate components, that is, the northwestern Pacific Ocean subtropical high (Li et al. 2012) and East Asian westerly jet (Li and Lin 2015). Higher prediction skill is seen in the years with strong ENSO forcing, because ENSO-related teleconnections generally can be better predicted by climate models (Kim et al. 2012). Recently a skillful prediction of summer precipitation over the Yangtze River valley is reported by using Met Office Global Seasonal Forecast System 5 (GloSea5), which arises from skillful prediction of rainfall in the deep tropics and around the "Maritime Continent" (Li et al. 2016). However, a study on seasonal drought predictability in China documented that the North American Multimodel Ensemble (MME) shows limited forecast skill for drought events over China and that drought predictability may rely on the impact of ENSO (Ma et al. 2015).

This study focuses on drought prediction over North China (box in Fig. 1), where the most frequent and longest duration of drought occurred in China (Zhang and Zhou 2015). The prediction of North China drought is greatly challenging because of its large climate variability modulated by both tropical and midlatitude climate systems. Several ingredients are proposed as predictors of North China drought. In the summer preceding El Niño peak phase, North China precipitation is suppressed as the combination of the Silk Road teleconnection and Pacific–Japan pattern (Wu et al. 2003; Zhang and Zhou 2012; Ding and Wang 2005; Ding et al. 2011), and the associated mechanisms have been illustrated. A prolonged spring–summer drought over North China tends to occur when La Niña transitions to El Niño with a negative North Pacific Oscillation phase in preceding winter. In this case, a low-level anomalous cyclonic circulation over the North Pacific Ocean can persist from the preceding winter until summer through a "seasonal footprinting mechanism" (Zhang et al. 2018). In addition, an extreme drought event, like the 2014 North and Northeast China summer drought, could be a joint result of many factors, such as the Pacific sea surface temperature anomalies (SSTA), Arctic sea ice anomalies, and warming over the European continent and Caspian Sea (Wang and He 2015). Wang et al. (2017) also demonstrated the importance of the combination of El Niño and Eurasian spring snow cover reduction. So far, the previous studies mainly focused on the prediction of a specific event. The predictability of North China summer drought is still unclear. The aim of this study is to explore the seasonal predictability of North China summer drought by comparing observation with hindcasts of the "ENSEMBLES" multimodel forecast and then to investigate the sources of predictability.

The remainder of the paper is organized as follows: section 2 describes the data and method. In section 3, the predictability of summer drought events in China with a 1-month lead is presented. The sources for the predictability are examined in section 4, and a summary and discussion are provided in section 5.

2. Data and method description

a. Seasonal hindcasts and validation data

The seasonal hindcasts used in this study are from the multimodel system in the ENSEMBLES seasonal–annual forecast in stream 2 (Weisheimer et al. 2009). Five global coupled atmosphere–ocean climate models participated in the multimodel forecast system, including the models from the Met Office, Météo France, the European Centre for Medium-Range Weather Forecasts, the Leibniz Institute of Marine Sciences at Kiel University, and the Euro-Mediterranean Centre for Climate Change in Bologna, Italy. For each year, the reforecasts for seven months with nine members of each model started on 1 February, 1 May, and 1 August. Details about model information and seasonal forecasts can be found in Weisheimer et al. (2009). The hindcasts covering the period 1960–2005, and 1961–2005 are selected here to keep consistent with the coverage of observational datasets. The prediction of North China summer [June–August (JJA)] drought starting on 1 May is examined in this study.

The validation datasets used in this study include 1) "CN05.1," which is a gridded precipitation and surface temperature dataset that is based on ~2400 observational stations over China and has a horizontal resolution of 0.5° × 0.5° (Wu and Gao 2013); 2) National Centers for Environmental Prediction–National Center for Atmospheric Research reanalysis data (Kalnay et al. 1996); 3) Hadley Centre Sea Ice and Sea Surface Temperature dataset, version 1 (HadISST1; Rayner et al. 2003); and 4) the precipitation reconstruction data compiled by the

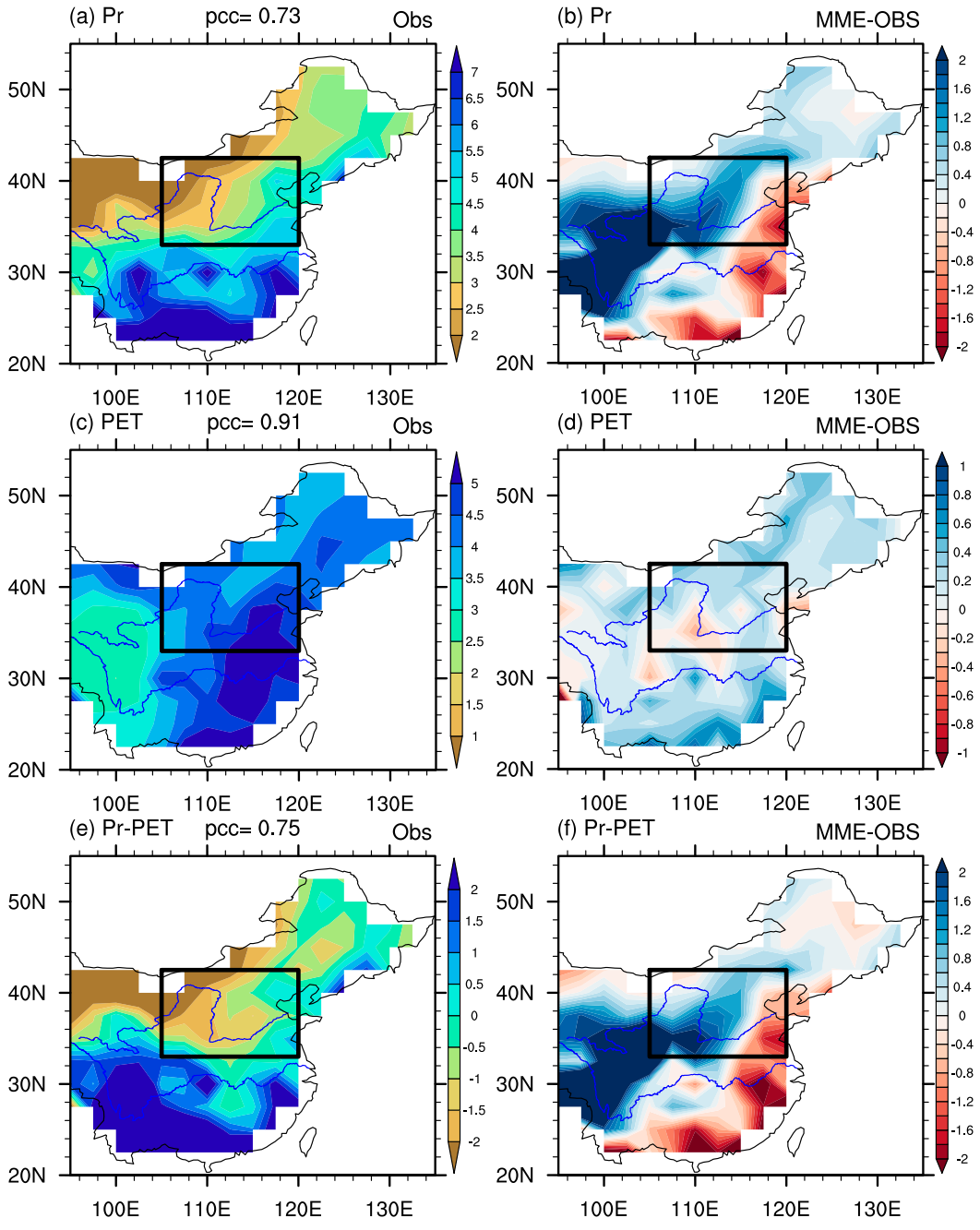

FIG. 1. The observed climatological summer (June–August) mean of (a) precipitation (mm day^{-1}), (c) PET (mm day^{-1}), and (e) difference between precipitation and PET (mm day^{-1}). (b),(d),(f) As in (a), (c), and (e), but for the bias of the MME of 45 members. The black-outlined box shows the target region of North China. The numbers over (a), (c), and (e) show the pattern correlation coefficients (label pcc) between MME and observations.

Climate Prediction Center at the National Centers for Environmental Prediction (PREC; Chen et al. 2002).

b. *Drought indices*

Two drought indices, standardized precipitation evapotranspiration index (SPEI; Vicente-Serrano et al. 2010) and standardized precipitation index (SPI; McKee et al. 1993), for the 3-month period from June to August are used to measure drought intensity. The standardization step is based on a nonparametric approach proposed by Hao et al. (2014) in which the probability distributions are empirically estimated. Because monthly

climatic balance between precipitation and potential evapotranspiration (PET) is considered in SPEI, the biases of precipitation and temperature in a seasonal forecast may introduce systematic bias in the forecast water balance and affect the prediction of SPEI. Thus, a simple bias correction on monthly precipitation and surface temperature is carried out following Turco et al. (2017) to ensure the climatological water balance is preserved. The PET is estimated with the Thornthwaite method (Thornthwaite 1948).

To remove the systematic bias in the mean value, the bias-corrected precipitation PR^* and surface temperature T^* for a given year by a member are derived by using the following equations (Turco et al. 2017):

$$T^* = T_f - (\langle T_f \rangle - \langle T_o \rangle) \quad \text{and}$$

$$PR^* = PR_f \times (\langle PR_o \rangle / \langle PR_f \rangle),$$

where f and o denote the model forecast and observation, respectively and angle brackets denote the climatology (mean) of precipitation or surface temperature in each member based on the whole hindcast period without the bias-correction year.

c. *Verification method*

As suggested by the Long Range Forecast Verification System of the World Meteorological Organization (http://www.bom.gov.au/wmo/lrfvs/), temporal correlation coefficient and relative operating characteristics (ROC) area skill score (ROCSS) at grid points based on the ROC diagram are used here to verify the deterministic and probabilistic forecast skill, respectively. When ROCSS is larger than 0.5, it means the hit rate (i.e., the relative number of times a forecast event actually occurred) is larger than the false-alarm rate (i.e., the relative number of times an event had been forecast but did not actually happen), indicating an effective prediction of a drought event.

3. Predictability of North China summer drought

The performance in forecasting the climate mean summer precipitation and PET is first examined (Fig. 1). The observed climatological summer precipitation in China shows a gradually decrease from southeast to northwest with the maximum rainfall exceeding 7 mm day^{-1} centered in South China and the south Tibetan Plateau and decreasing to 2 mm day^{-1} over Northwest China (Fig. 1a). Different from the precipitation, a zonal decrease from east to west is observed in climatological PET, with maximum (~6 mm day^{-1}) centered in the lower reaches of Yangtze River and minimum (~2 mm day^{-1}) centered in the Tibetan Plateau (Fig. 1c). The magnitude of PET over North China is higher than that of precipitation. Thus, the climatic water balance between precipitation and PET in summer shows a gain of water about south of 32°N and a loss of water north of 32°N (Fig. 1e). MME generally well predicted the spatial distributions of climatology summer precipitation and PET, with pattern correlation coefficients of 0.73 and 0.91 over the whole of China, respectively, suggestive of a better prediction of PET. For North China, a main deficiency in forecasting precipitation is an overestimation over the western part of North China (110°–115°E) and an underestimation over eastern North China (115°–120°E). Thus, an artificial gain or loss of water is forecast over the western or eastern part of North China, respectively (Fig. 1f). To avoid this systematic bias in climatology, a bias correction is carried out on the forecast precipitation and temperature in each member. The spatial distributions for the climatology of bias-corrected precipitation and PET are the same as observed (figures not shown).

The spatial distributions of the 1-month-lead seasonal forecast skills for summer mean SPEI, SPI, precipitation, and PET in terms of correlation coefficient at each grid point for 1961–2005 are shown in Fig. 2. A statistically significant correlation of forecast SPEI with observations is shown over North China, reaching 0.5 at maximum over the northwestern corner of North China (35°–42°N, 105°–113°E). A compared with SPEI, a positive correlation coefficient between forecast SPI and observation is seen over North China, and it is statistically significant at the 10% level over central North China (32°–42°N, 110°–115°E) (Fig. 2b), demonstrating that skillful prediction of both rainfall and temperature contributes to the high correlation of SPEI over North China (Figs. 2c,d).

The time series of the observed and forecast drought indices area averaged over North China are shown in Fig. 3. ENSEMBLES forecasts well the temporal changes of SPEI, SPI, precipitation and PET over North China despite a large model spread, with the correlation coefficients against observation reaching 0.49, 0.39, 0.44, and 0.63, respectively, all statistically exceeding the 5% significance level. The drought years over North China, particularly the prolonged drought events from 1999 to 2002, are well predicted by the MME (Figs. 3a,b). A decadal variation and long-term trend of PET over North China is observed for 1961–2005, with negative PET anomalies before 1998 and positive PET anomalies afterward. Note that ENSEMBLES fails to predict the precipitation deficit in 1999; thus the predicted negative SPEI in 1999 is caused by a good prediction of extremely high PET. We further examined the results by removing

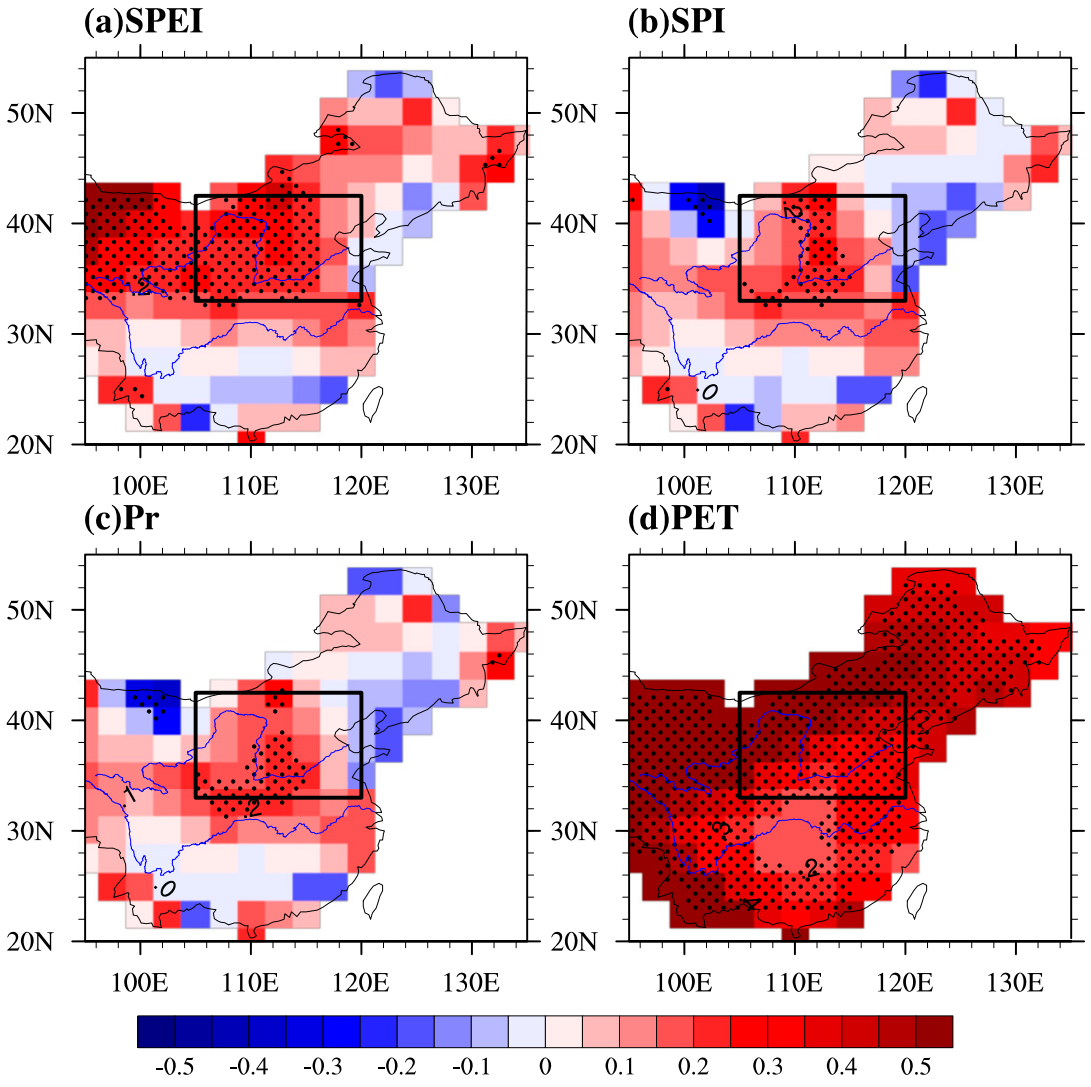

FIG. 2. The temporal correlation coefficients for 1961–2005 between the observed and 1-month-lead prediction of MME for (a) SPEI, (b) SPI, (c) precipitation, and (d) PET at each grid. The dotted areas are statistically significant at the 10% level using *t*-test. The black-outlined box shows the target region of North China.

the long-term linear trend and interdecadal variations with periods longer than 9 yr using a high-pass Lanczos filter. The statistically significant correlation coefficients can still be found, except with a reduction in PET from 0.63 to 0.47. The correlation coefficients for the interannual variability of area-averaged SPEI, SPI, and precipitation are 0.43, 0.38, and 0.44, respectively—comparable to the original ones. This demonstrates that the prediction skill for North China drought, particularly defined by SPEI, SPI, and precipitation, is not highly influenced by the interdecadal variability or warming trend. Therefore, we will use the original data in the following discussion.

To further verify the predictability of North China drought, the spatial distributions of ROCSS for the probabilistic forecast of drought event defined by SPEI ≤ -1 and SPI ≤ -1 (threshold for moderate drought events) are shown in Figs. 4a and 4b. The ROCSS for drought event defined by SPEI is larger than 0.5 over most region of North China, whereas when defined by SPI the ROCSS exceeding 0.5 is only seen over its western part (Figs. 4a,b). Given that drought is associated with precipitation deficit and higher PET, we further examined the ROCSS of a below-normal event of precipitation and an above-normal event of PET (Figs. 4c,d). Here, a below-normal or above-normal event is defined as respectively being in the driest or

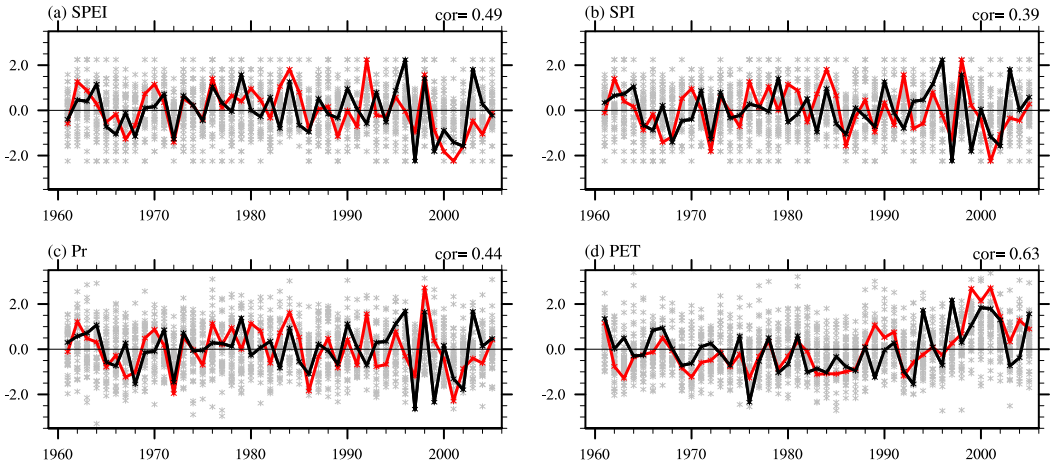

FIG. 3. Standardized time series of regional averages over North China (33°–41.5°N, 105°–120°E; box in Fig. 2) for (a) SPEI, (b) SPI, (c) precipitation, and (d) PET. Black and red lines denote observations and MME, respectively, and gray asterisks denote each member. The correlation coefficient between observations and MME for 1961–2005 is shown in the top-right corner of (a)–(d).

warmest one-third among 1961–2005. The ROCSS for a below-normal precipitation event and above-normal PET are both still higher than 0.5 over North China, indicating an effective prediction of North China summer drought events.

4. Sources of predictability for North China summer drought

The above analysis demonstrates a skillful prediction of summer drought over North China led by 1 month. Because precipitation deficit is the main cause of negative SPEI and SPI in drought years across the whole period, this section will investigate the sources of predictability for North China summer drought by examining the large-scale circulations associated with less precipitation.

According to the time series of SPEI as shown in Fig. 3a, the summer drought years of North China with SPEI ≤ -1.0 are selected. They are 1968, 1972, 1986, 1997, 1999, 2001, and 2002. The composite distributions of SPEI and SPI for the drought years both in the observations and MME hindcasts are shown in Fig. 5. The dry condition in observations as defined by both SPEI and SPI is well forecast by MME but with a westward shift of the drought center, leading to a reduction in reliability over 105°–110°E, 35°–40°N. The probability of drought events is higher than 60% as seen from the model consistency, demonstrating a high model consistency in forecasting the summer drought events of North China.

The composite summer mean precipitation and associated circulation anomalies for the drought years are first examined (Fig. 6). In the observations, significant rainfall deficit is shown over North China, reaching $-1.2\,\mathrm{mm\,day^{-1}}$ over eastern North China (Fig. 6a). Models well capture the significant dry condition over the whole of North China (Fig. 6b), with a weaker magnitude ($\sim -0.4\,\mathrm{mm\,day^{-1}}$ in maximum) and a westward-shifted dry center. In the observations, two key circulations are shown, that is, a significant northwestern Pacific cyclonic circulation anomaly (NWPCCA) at lower levels, confined to south of 30°N, and an upper-troposphere temperature (UTT) cooling over East Asia (20°–40°N, 80°–140°E). The latter circulation is associated with a cyclonic circulation anomaly to the south of a westerly jet and an anomalous anticyclone to the north at the upper level. Consequently, the East Asian continent is dominated by a significant higher sea level pressure (SLP) centered on Mongolia (Fig. 6c). The northerly wind anomaly of the east flank of the anticyclonic circulation anomaly over East Asia joins the northerly anomaly associated with the NWPCCA, leading to a weakened East Asian summer monsoon and reducing the water vapor transport from the ocean to North China (Fig. 6c). A reasonable prediction of the two key circulations can be found in MME, particularly the NWPCCA and its baroclinic structure (Figs. 6d,f). The East Asian UTT cooling is partly predicted by MME, with a statistically significant cyclonic circulation anomaly over central China at 200 hPa. The positive SLP anomalies from Mongolia to northeastern Asia are predicted but are statistically insignificant. The northerly wind anomalies along the East Asian coast are also shown in MME but are much more southward shifted, leading to less water vapor transport

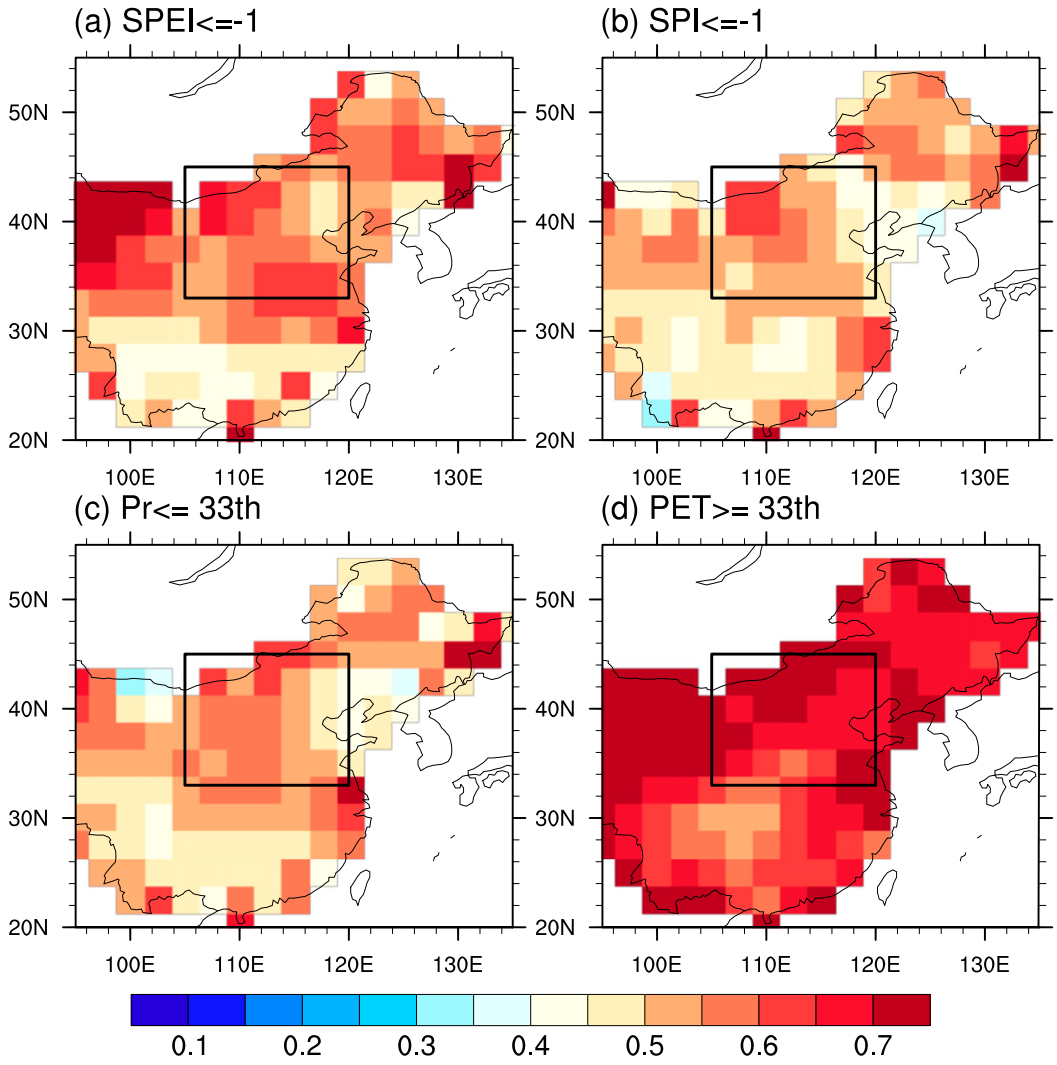

FIG. 4. Spatial distribution of ROCSS for the probabilistic forecast of a drought event defined by (a) SPEI ≤ -1.0 and (b) SPI ≤ -1.0. (c),(d) As in (a) and (b) but for the below-normal precipitation events and above-normal events of PET, where a below- or above-normal event is respectively defined as being in the driest or warmest one-third among 1961–2005.

to North China. We notice that both the low-level northerly anomaly and the upper-level UTT cooling are westward shifted relative to the observation, contributing to the westward shift of the dry center in the predictions.

To investigate the role of the two key circulations in North China drought, we selected the driest and wettest members from all predictions of each drought event with the area-averaged SPEI ranked as the bottom 15% and top 15%, respectively, and termed them the high-skill group and low-skill group in predicting North China drought. There are 49 members in each group, and the corresponding composite results are shown in Fig. 7. Significant dry and wet conditions over North China are predicted in the high-skill and low-skill groups, respectively (Figs. 7a,b). The NWPCCA exists in both groups, except that it is stronger and more northward extended in the high-skill group. The main difference between the two groups can be found over midlatitudes, where there is a UTT cooling over central China in the high-skill group but a warming over East Asia in the low-skill group (Figs. 7e,f). They correspond to higher SLP and lower SLP over China, respectively (Figs. 7c,d). Thus, significant northerly winds along the East Asian coast are predicted in the high-skill group, resulting in less rainfall over North China, although it is not as far northward as the observations (Fig. 7c). In contrast, in the low-skill group, the lower SLP over western China

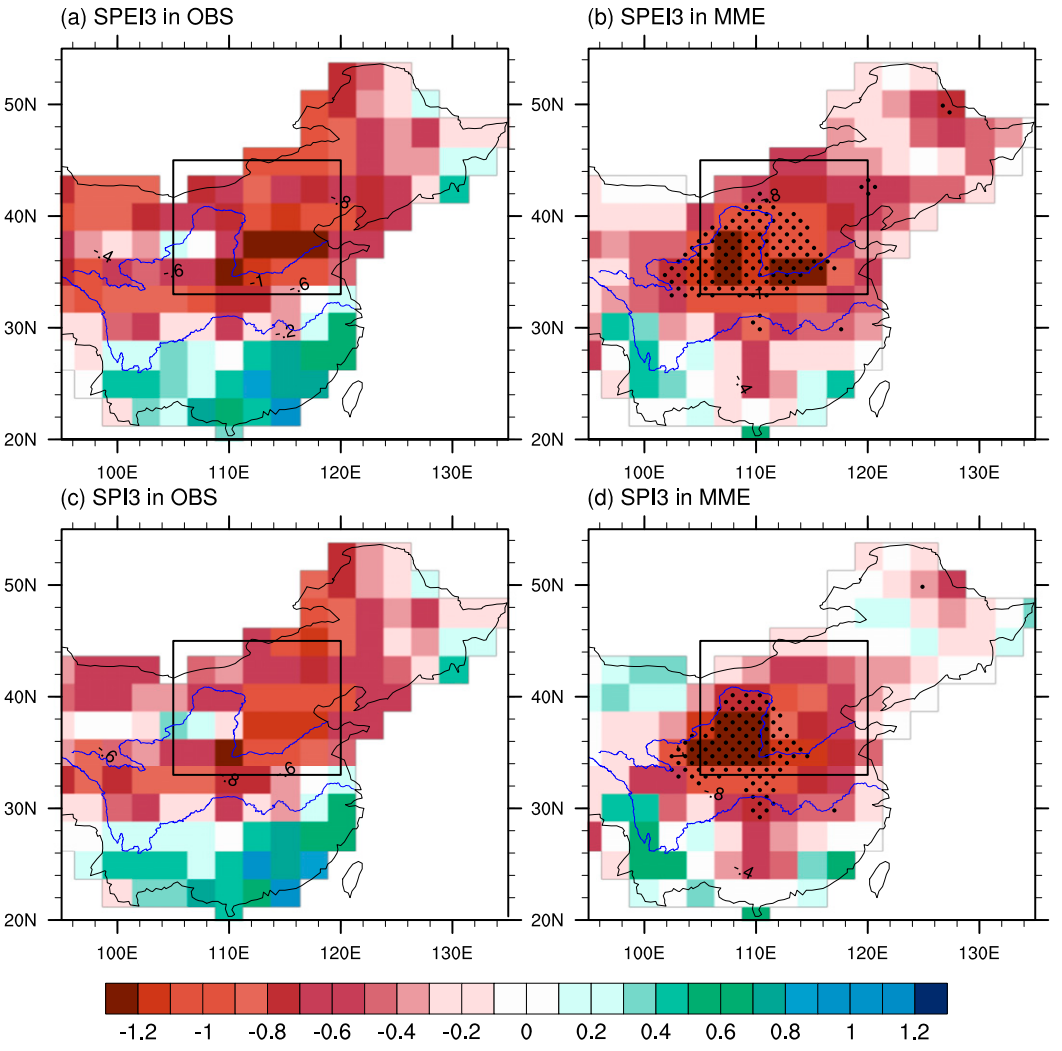

FIG. 5. Composite drought indices of the years with SPEI less than −1.0 for (a),(b) SPEI and (c),(d) SPI in (left) the observations and (right) MME. Dotted areas in (b) and (d) denote exceeding 2/3 of the members forecasting a dry condition.

joins in the NWPCCA, leading to a farther-westward NWPCCA (Figs. 7d,f). So, no significant northerly anomalies are predicted along the East Asian coast, and more water vapor transport from the North Pacific Ocean to North China is predicted, leading to excessive rainfall over North China in the low-skill group. The difference between the two groups indicates that models have a skillful prediction of the NWPCCA but limited skill for East Asian UTT.

A scatterplot of North China summer rainfall with East Asian UTT anomalies and NWPCCA for each drought event is further shown in Fig. 8. In the observations (dots in Fig. 8), five of the seven drought events are associated with negative values of UTT (except 1972 and 1999), and six with NWPCCA (except 1999). To reduce the uncertainty caused by initial conditions, we use the ensemble mean of an individual model for any given drought event to show the prediction result of that model. There are 6 predictions for a given event when MME is included. For the selected seven droughts, there are 42 predictions in total. 79% of the 42 predictions show precipitation deficit over North China, verifying the high consistency among models as shown in Fig. 5. For the drought years, positive correlations of North China summer precipitation with the East Asian UTT anomaly ($r = 0.43$) and NWPCCA ($r = 0.43$) can be seen from the predictions (Fig. 8), respectively, both statistically significant at the 5% level, demonstrating a close contribution of the two key large-scale circulations to North China summer droughts in prediction. For the 42

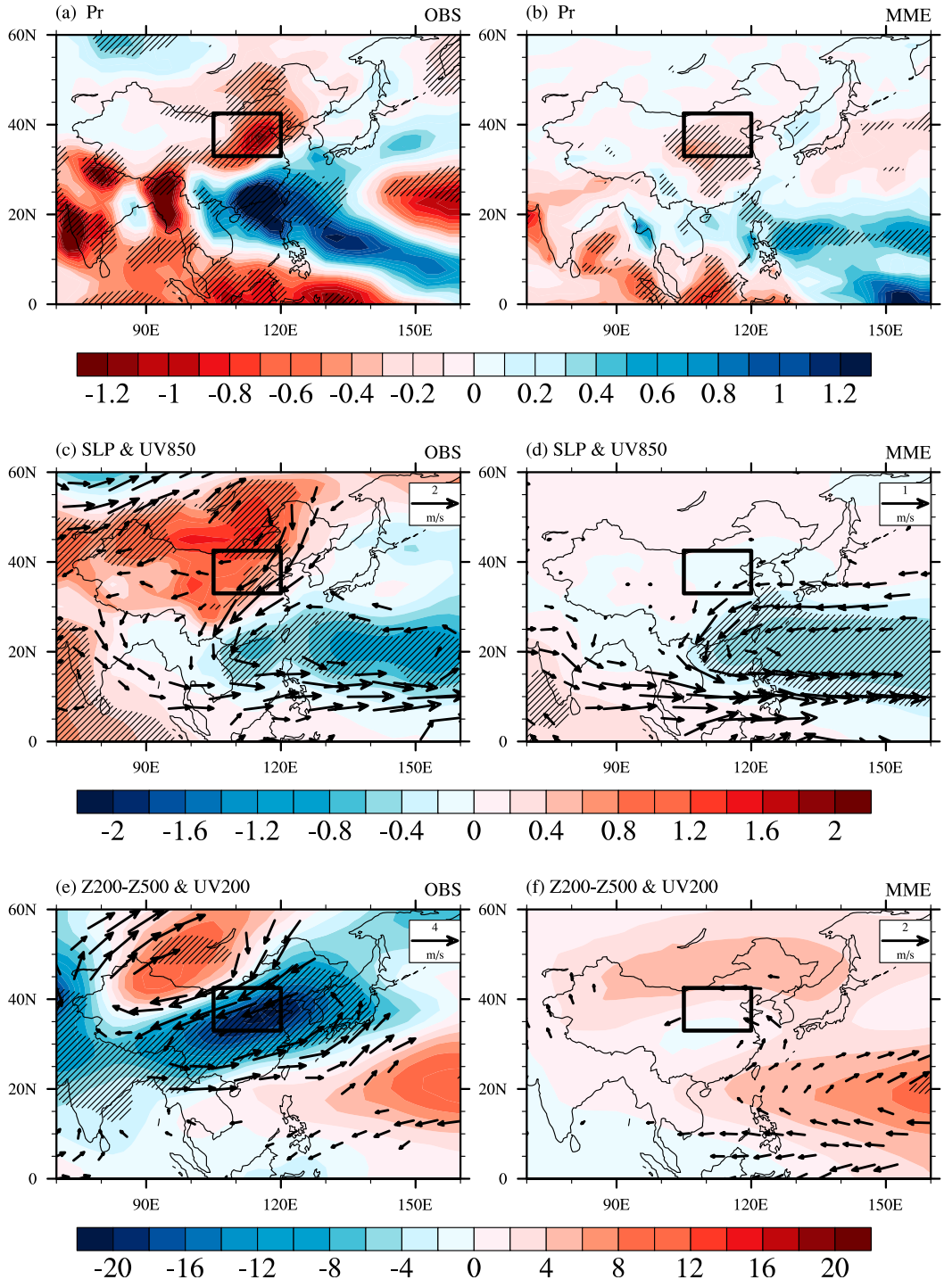

FIG. 6. Composite circulation anomalies of the North China summer drought years in (left) the observations (right) MME for (a),(b) precipitation (mm day^{-1}); (c),(d) SLP anomalies (shading; hPa) and 850-hPa wind anomalies (vectors; m s^{-1}); and (e),(f) anomalies of 200-hPa winds (vectors; m s^{-1}) and 200–500-hPa thickness (shading; m), which is defined as the geopotential height difference between 200 and 500 hPa (label Z200–Z500). Wind-anomaly vectors that are statistically significant at the 10% level using the Student's *t* test are shown, and the shading variables that are statistically significant at the 10% level are denoted by the hatched areas.

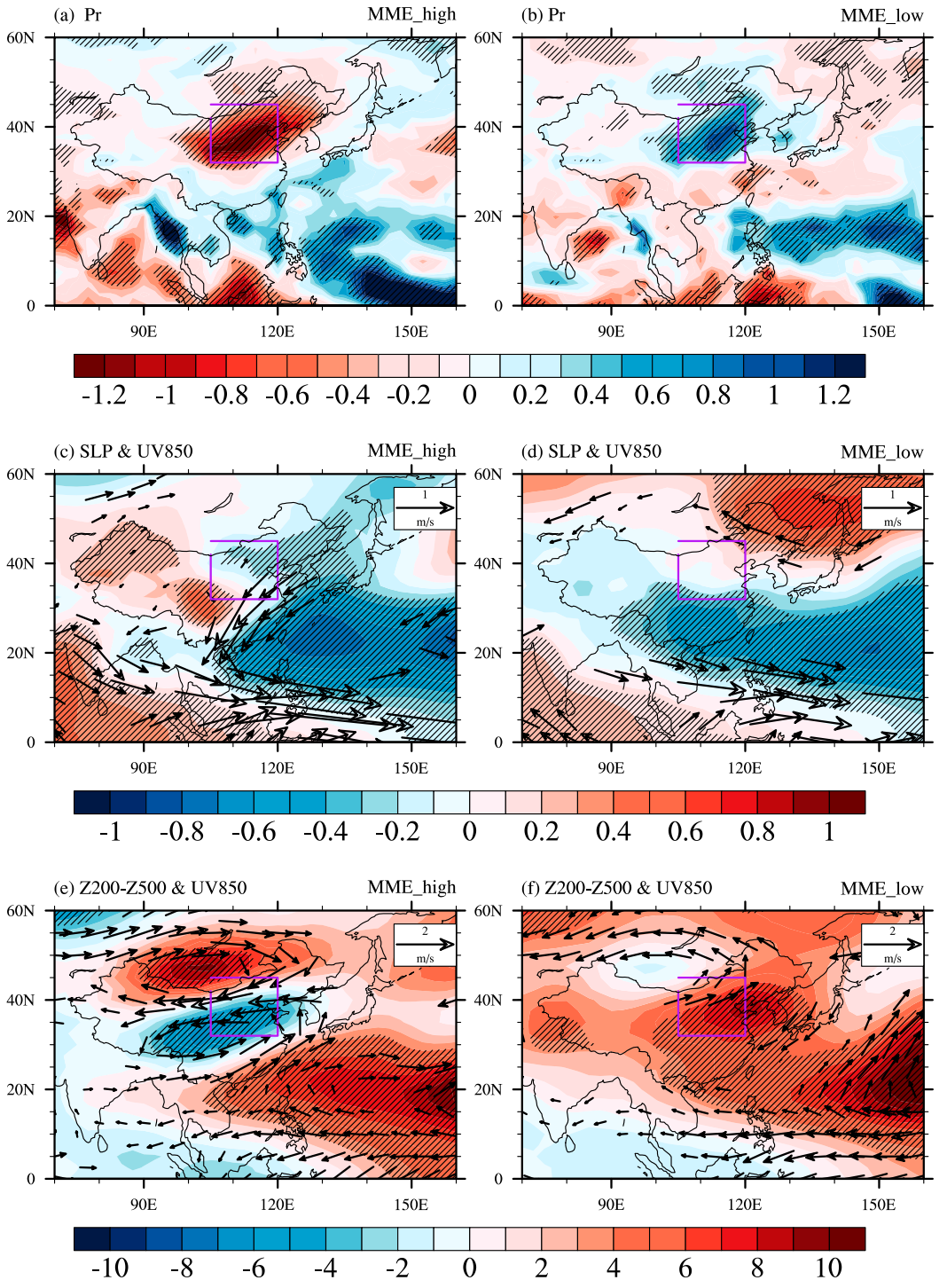

FIG. 7. As in Fig. 6, but for the composite circulation anomalies of the (left) high-skill members and (right) low-skill members in predicting North China drought. The first 15% driest and wettest members from the 45 members for each drought event based on the SPEI averaged over North China are selected and respectively termed as high- and low-skill members in predicting North China drought.

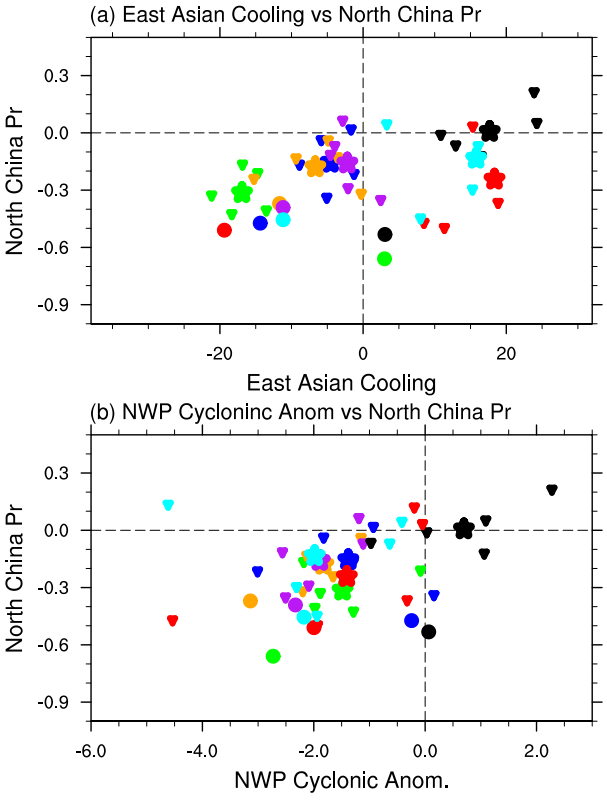

FIG. 8. Scatterplots showing the relationship between summer precipitation anomalies (mm day^{-1}) averaged over North China and crucial circulations for (a) East Asian UTT anomalies (m) and (b) NWPCCA (m s^{-1}), where the y axis is the precipitation anomalies and the x axis is circulation anomalies. East Asian UTT anomaly is defined as Z200–Z500 averaged over 25°–42°N, 100°–130°E. NWPCCA is defined as the wind shear of zonal wind at 850 hPa between 25°–35°N, 100°–150°E and 5°–15°N, 90°E–180°. Dots, stars, and triangles denote the observation, MME, and ensemble mean of each model, respectively. Blue, green, orange, purple, black, red, and cyan represent the North China drought year 1968, 1972, 1986, 1997, 1999, 2001 and 2002, respectively.

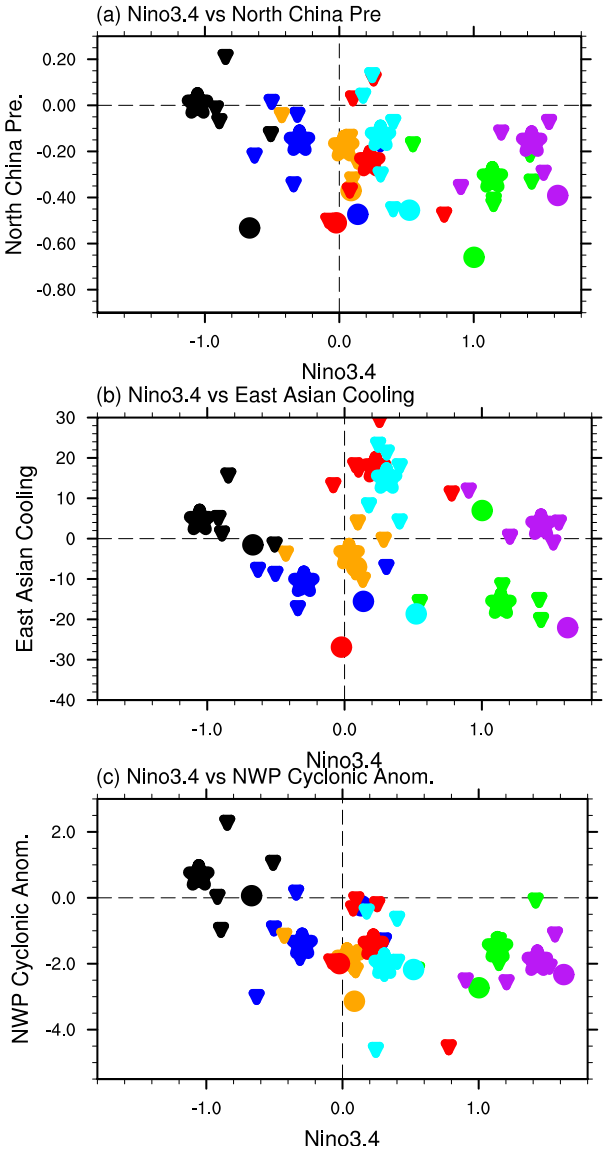

FIG. 9. As in Fig. 8, but for scatterplots showing the relationship of Niño-3.4 index (x axis; °C) with summer precipitation anomalies averaged over North China and the two crucial circulations (y axis) for (a) summer precipitation over North China (mm day^{-1}), (b) East Asian UTT anomalies (m), and (c) NWPCCA (m s^{-1}).

predictions, the ratio of NWPCCA is 86% when 1999 is included and 97% when it is excluded, while the number of negative East Asian UTT (55%) is only slightly higher than that of positive value (45%). When including all years 1961–2005, significant correlation coefficients of North China summer precipitation with East Asian UTT ($r = 0.28$) and NWPCCA ($r = 0.40$) for 1961–2005 are also obtained, indicating the importance of the two circulation anomalies for North China drought in the observations. However, only the positive correlation between North China summer precipitation and NWPCCA can be predicted by MME, with a correlation coefficient at 0.48 for 1961–2005. It further demonstrates a better skill for NWPCCA than the East Asian UTT cooling associated with North China summer drought.

El Niño is one of the main drivers of North China summer drought. The relationship of ENSO with North China summer precipitation and the two key circulation anomalies is examined and shown in Fig. 9. A negative correlation between Niño-3.4 and North China summer rainfall is obtained from the 42 predictions (Fig. 9a). In terms of the relationship between the two large-scale circulation anomalies, only the NWPCCA is statistically significant related with Niño-3.4 (Fig. 9c), and there is no obvious correlation between East Asian UTT and Niño-3.4 (Fig. 9b). Thus, the predicted ENSO exerts its impact

on North China summer precipitation mainly through modulating the NWPCCA. Seeing from the magnitude of Niño-3.4, only those for 1972 and 1997 exceed 0.5°C. Those two summers were both before the peak phase of eastern Pacific (EP) El Niño, so they are regarded as well-established EP El Niño in summer here. The NWPCCA and UTT cooling in those two years can be both well predicted. However, the remaining events are not associated with strong EP El Niño SSTA in summer. Because 1999 was a strong La Niña year, the dry North China in 1999 is beyond the relationship between ENSO and North China rainfall. Thus, in the observations, the UTT cooling and NWPCCA are both absent for the 1999 drought events, and they are not well forecast by ENSEMBLES. So we will exclude the 1999 drought event in the following discussion. The mechanisms in the drought events with and without well-established EP El Niño SSTA in summer will be investigated separately.

The composite summer circulation anomalies for the two drought events with strong EP El Niño events are shown in Fig. 10. The impact of the El Niño developing phase on the East Asian summer monsoon, specifically on the NWPCCA and East Asian UTT cooling, has been well illustrated (Wu et al. 2003; Chou et al. 2003; Zhang et al. 2018; Wen et al. 2018). In the case of the two drought events discussed here, a well-established horseshoe pattern of the EP El Niño SSTA is clearly shown in the observations, with the equatorial EP 2.0°C warmer than the normal. Forced by the El Niño SSTA and enhanced convection over the equatorial central Pacific (CP), the Walker circulation is weakened, resulting in less rainfall over the Maritime Continent and India (Fig. 10a). As a Gill–Matsuno response to the enhanced CP equatorial convection, the NWPCCA is triggered (10°–30°N, 100°–160°E) and further propagates northward with an anticyclone anomaly over South Japan and a cyclone over Northeast China. This meridional wave train is the so-called Pacific–Japan (PJ) pattern (Nitta 1987; Huang and Sun 1992), with a baroclinic structure over the central China (Kosaka and Nakamura 2010). An upper-level Rossby wave train is seen along the Asian westerly jet due to less latent heat forcing over India, and it further contributes to the cooling over Northeast China (Fig. 10c). This upper-level wave train is the so-called Silk Road teleconnection, and it is a regional feature of circumglobal teleconnection in boreal summer (Enomoto et al. 2003; Ding and Wang 2005; Ding et al. 2011). An equivalent barotropic structure exists in all circulation centers over the midlatitude Eurasian continent but the one over the Mediterranean–central Asia, which is due to the influence of diabatic heating associated with Indian monsoon precipitation. The lower-level cyclonic anomaly over Northeast China is also a part of the Silk Road teleconnection. The combination of Silk Road and PJ teleconnections leads to the anomalous northerly along the East Asian coast and anomalous descent over North China. The observed Silk Road teleconnection, PJ pattern, and associated precipitation forcing during well-established EP El Niño summer are all well predicted by MME, although with less magnitude at the mid–high latitudes (Figs. 10b,d,f). Thus, models show a reasonable prediction of the summer drought over North China. However, in comparing with those for all drought events as shown in Fig. 6, it is seen that the UTT cooling is shifted northeastward and the NWPCCA is located more southward (Figs. 10c,e).

The composite summer circulation anomalies for the drought events without well-established EP El Niño are shown in Fig. 11. Significant SST warming spanning from the central equatorial Pacific to subtropical North Pacific (10°N, 150°E–150°W) is seen in the observation, similar to the CP El Niño SSTA pattern. All of the four drought summers were the year before CP El Niño except 2001 (Yu et al. 2012). Enhanced convection over the central equatorial Pacific and rainfall deficit over India associated with weakened Walker circulation are also observed (Fig. 11c), as well as the Silk Road teleconnection. Compared with the events associated with well-established EP El Niño, the upper-level cooling center over East Asia shifted southward to 30°N, and another wave train with a nearly equivalent barotropic structure is evident over the higher latitude of the Eurasian continent north of 50°N, which may contribute to the high-pressure anomalies over the East Asian continent (Fig. 11e). Another difference is seen from the magnitude and area of the NWPCCA, which becomes much stronger and reaches more northward (40°N) associated with CP El Niño SSTA (Fig. 11c). Previous literature documented that two possible mechanisms could contribute to the NWPCCA associated with CP El Niño. One is the same as that in the well-established EP El Niño, that is, a Gill–Matsuno response to the enhanced CP convection due to warm SSTA over central equatorial Pacific (He and Zhou 2014). The second mechanism is the coupled SST–surface wind interaction in the North Pacific through wind–evaporation–SST (WES) feedback associated with Pacific meridional mode (PMM) (Chiang and Vimont 2004; Yeh et al. 2015), which can sustain the NWPCCA from the preceding spring to summer with an equatorward extension; details of the mechanism will be discussed later.

In MME, the observed NWPCCA and CP warming are both well predicted (Figs. 11b,d,f). In contrast to the uniform SST warming over the CP in observations, MME exhibits a meridional SSTA gradient with the maximum

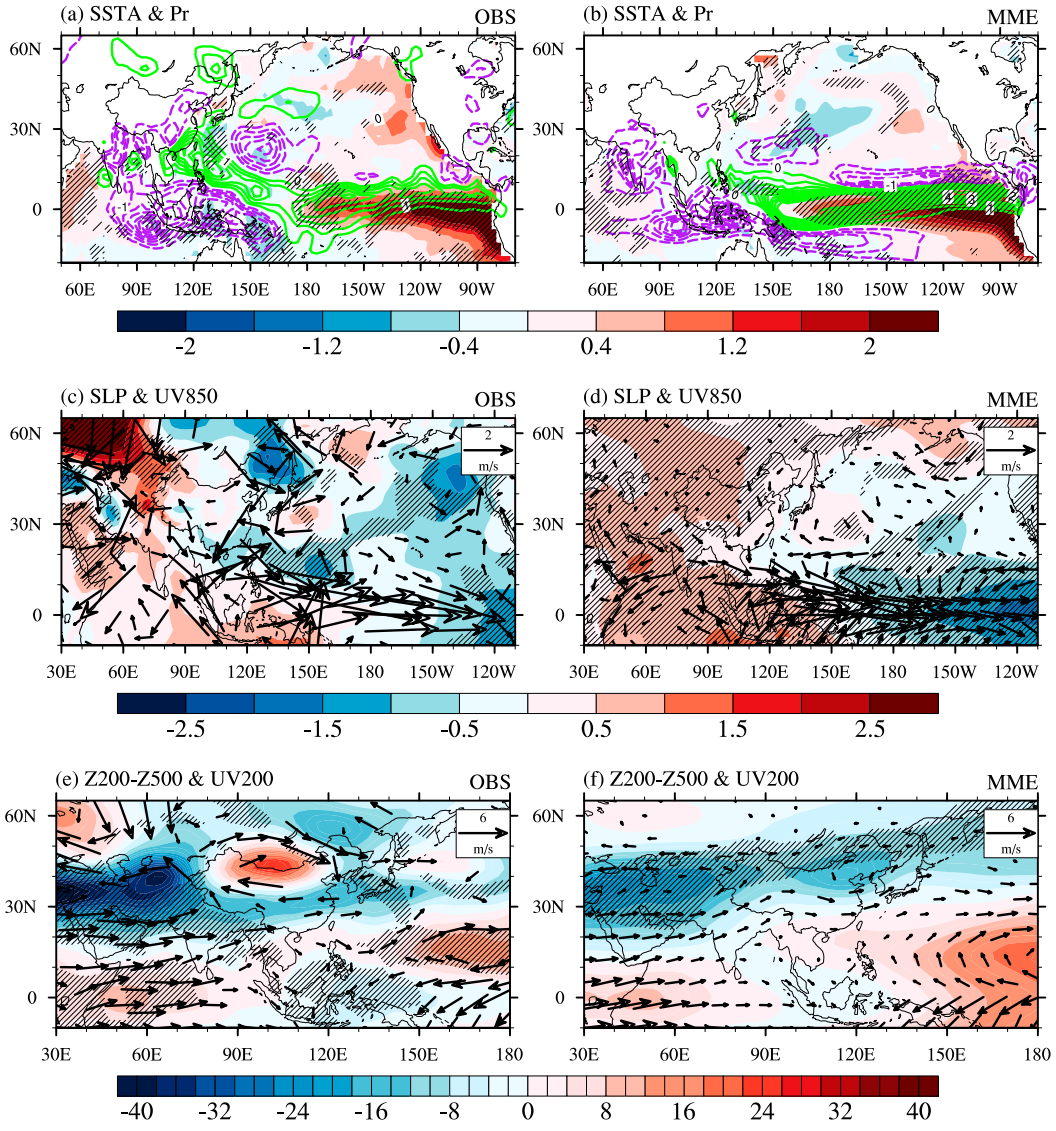

FIG. 10. Composite circulation anomalies of the two North China summer droughts associated with well-established EP El Niño for (left) observations and (right) MME for (a),(b) SST (shading; °C) and precipitation (contours; mm day^{-1}) anomalies; (c),(d) SLP (shading; hPa) and 850-hPa wind anomalies (vectors; m s^{-1}); and (e),(f) 200–500-hPa thickness (shading; m) and 200-hPa wind (vectors; m s^{-1}) anomalies. Wind-anomaly vectors that are statistically significant at the 10% level using the Student's t test are shown, and the shading variables that are statistically significant at the 10% level are denoted as hatched area.

warm SSTA over the subtropical central North Pacific (5°–20°N, 150°E–120°W) but relative weaker warming over the equator, indicating a slower warming of the equatorial CP or onset of CP El Niño in prediction. This meridional SSTA gradient in prediction leads to anomalous wind flow crossing from the equator to subtropical central North Pacific. Consequently, anomalous convergence and divergence is predicted over the subtropical central North Pacific and equatorial CP, respectively (Figs. 11b,d), resulting in significantly enhanced convection over subtropical central North Pacific but less rainfall over the equatorial CP (Fig. 11b). The NWPCCA in MME is a Gill–Matsuno response to the more latent heating over the subtropical central North Pacific. As the heating intensity is stronger than observation and located north of the equator, the predicted NWPCCA extends much more northward and eastward than the observation. The failure in predicting the enhanced convection over the CP demonstrates a failed prediction of the weakened Walker circulation, and the suppressed

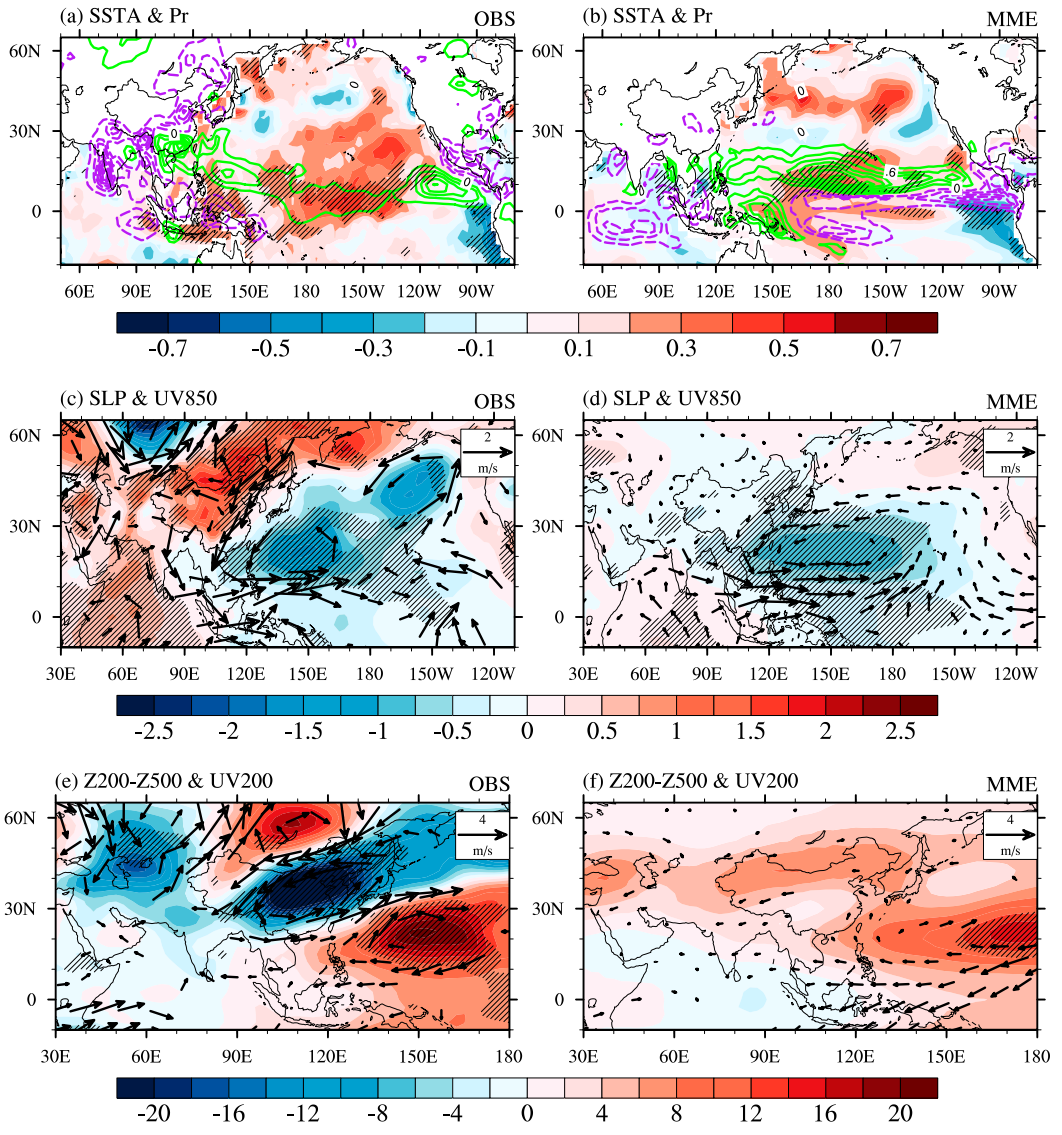

FIG. 11. As in Fig. 10, but for the circulation anomalies for the four drought years without well-established El Niño in summer.

rainfall over the Maritime Continent and India is much weaker than the observation. As a result, the Silk Road teleconnection and associated East Asian cooling are absent in MME (Figs. 11d,f). We also notice that the midlatitude North Pacific SST along the 40°–50°N in MME is above normal, opposite to the observations (Figs. 11a,b). This warm extratropical SSTA may increase the Eurasian UTT by affecting the displacement of the jet stream and setting up a quasi-stationary wave (Chattopadhyay et al. 2015). So, the failure in predicting the midlatitude North Pacific SSTA may be another possible reason for the warm UTT over the Eurasian continent in prediction. The above comparison indicates that the reasonable prediction of North China drought without well-established El Niño in summer is mainly due to the reasonable prediction of the NWPCCA. The ENSEMBLES models have little ability in predicting the related midlatitude atmosphere activities.

To understand the source of predictability for NWPCCA and slower warming of the central equatorial Pacific, the evolution of SSTA and associated circulation anomalies in the preceding spring in both observation and prediction are examined and shown in Fig. 12. Since the prediction in this study started on 1 May, the SSTA in April is used as the initial condition here. In general, a persistence of the NWPCCA from April to May is observed in the selected drought years, and it is associated with an equatorward and westward development of

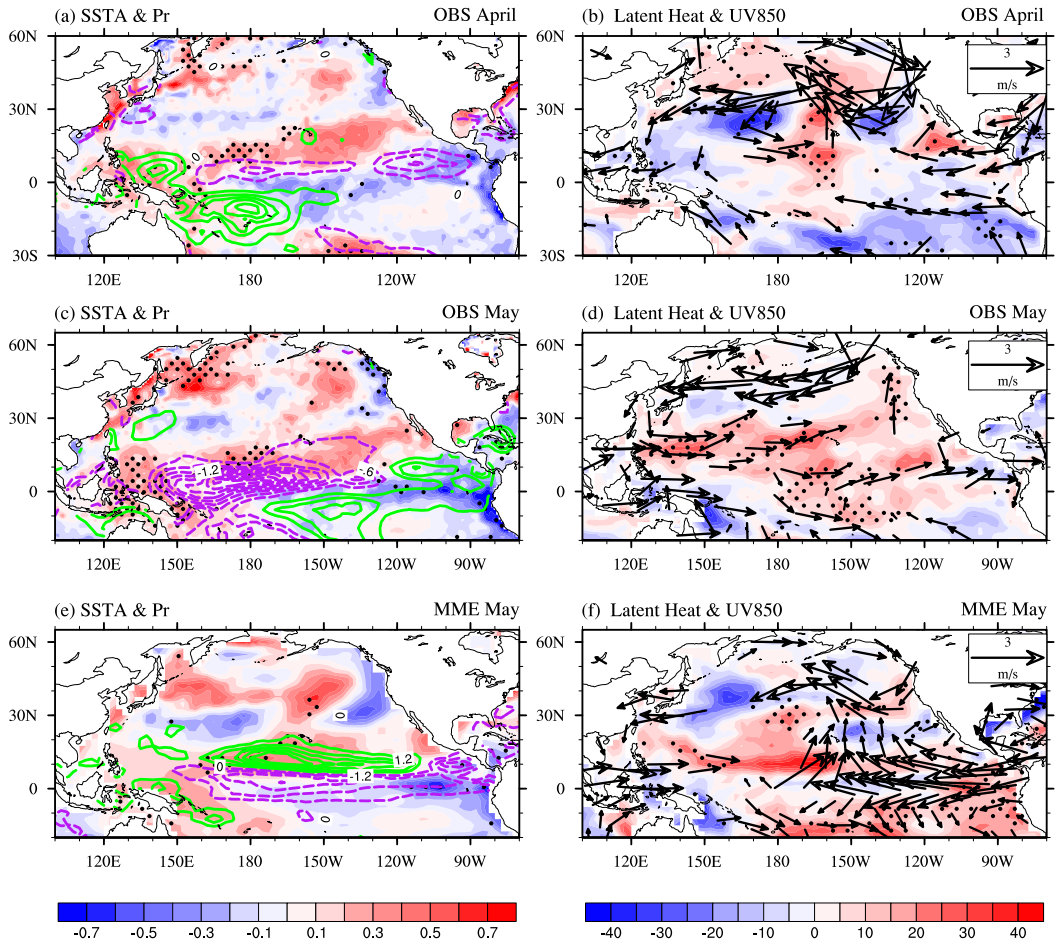

FIG. 12. Evolution of (left) SST (shading; °C) and precipitation (contours; mm day^{-1}) anomalies and (right) 850-hPa wind (vectors; m s^{-1}) and latent heat flux (W m^{-2}; positive means downward) anomalies from April to May associated with droughts without well-established EP El Niño for (a),(b) April observations, (c),(d) May observations, and (e),(f) May MME. Only vectors that are statistically significant at the 10% level are shown in (a) and (b). The dots denote that the shaded variables are statistically significant at the 10% level using the Student's *t* test.

warm SSTA over the North Pacific Ocean. In the initial month (Fig. 12a), a meridional dipole SSTA pattern, that is, PMM, is observed over the tropical Pacific Ocean with warm anomalies over subtropical central North Pacific and cold ones along the equatorial EP (Fig. 12a). On one hand, the westerly winds associated with NWPCCA in April result in a relaxation of the lower-level trades and less upward evaporation from ocean to atmosphere (Fig. 12b) and a positive feedback on the original SST anomalies. The SSTA over the central North Pacific gets warmer in May (Fig. 12c) (Vimont et al. 2001, 2003a,b; Chiang and Vimont 2004; Alexander et al. 2010). On the other hand, the surface warming over the subtropical central North Pacific lowers in situ atmosphere pressure and induces anomalous southwesterly winds to the southern plank of the anomalous region and northeasterly wind to its northern plank, further maintaining the NWPCCA (Vimont et al. 2009; Wu et al. 2010). The westerly anomalies reach the equator in May (Fig. 12d), and the WES feedback warms up the equatorial SST leading to CP warming in JJA (Fig. 11a). Note that the equatorial CP (5°S–5°N, 180°–150°W) in May is dominated by suppressed rainfall due to divergence from the equator to the subtropical central North Pacific (Fig. 12c). Thus, the equatorial central Pacific Ocean gets more shortwave radiation flux, which also contributes to the CP warming (figures not shown).

As for the processes in prediction, in response to the initialized dipole SSTA pattern in April, the anomalous gradient across the equator forces anomalous winds flowing from cold water toward warm water (Fig. 12f). In accord with the Coriolis force, anomalous southwesterly winds prevail along the southern flank of the warm

SSTA, leading to less upward evaporation over the subtropical central North Pacific (Fig. 12f) and warm SSTA over the subtropical central North Pacific, enhancing the local convection and increasing precipitation (Fig. 12e). A cyclonic circulation anomaly, that is, NWPCCA, is predicted to the northwest of the enhanced convection, indicating a good prediction of the persistence of the NWPCCA from April to May. The predicted westerly anomalies have not arrived at the equatorial CP, which is still dominated by easterly anomalies. Thus, the convection over the central equatorial Pacific is suppressed, leading to less latent heat warming (Fig. 12f) but more shortwave radiation. Then the equatorial Pacific SST warming rate is slower than observations (Fig. 12f), and the meridional SSTA pattern in spring persists to summer (Fig. 11b).

5. Summary and discussion

This study investigates the seasonal prediction skill of North China summer drought in the ENSEMBLES multimodel seasonal forecast system in stream 2 starting on 1 May. This study shows a skillful prediction of North China summer drought in ENSEMBLES for 1961–2005. The correlation coefficient of predicted SPEI/SPI with observation is 0.49/0.39, statistically significant at the 5% level. The summer precipitation and temperature averaged over North China are both reasonably forecast, with correlation coefficients for 1961–2005 reaching 0.44 and 0.63, respectively. ROC analysis indicates that the forecasts can distinguish a drought event over North China from a nondrought event. Seven extreme summer drought events over North China are selected from 1961 to 2005, and all of them are predicted as drought events. The deficits in summer precipitation are all well predicted in ENSEMBLES, except 1999 drought event.

The NPWCCA at lower levels and East Asian UTT cooling are proposed to be the two key large-scale circulations responsible for the North China summer drought. An examination of the two key circulations for all drought events shows a reasonable prediction of NWPCCA, with high model consistency, whereas there is a large spread in East Asian UTT cooling. Two sources of predictability are identified in this study. The first one comes from the PJ pattern and Silk Road teleconnections forced by well-established EP El Niño SSTA in summer. The NWPCCA is the south cell of the PJ pattern located south of 30°N, and East Asian UTT cooling is a regional feature of the Silk Road teleconnection centered over Northeast China. Models can predict well the strong EP El Niño SSTA and associated two teleconnections, and thus they show a good prediction of North China summer drought.

The other prediction source is from the warm SSTA over the CP associated with CP El Niño developing. Compared to the drought events with well-established EP El Niño, the NWPCCA is much stronger and more northward shifted, and the East Asian UTT cooling dominates the whole of China and is associated with significant impacts from the mid–high-latitude atmospheric anomalies. In MME, the prediction skill on drought is from a skillful prediction of the persistence of NWPCCA. The East Asian UTT cooling is insignificant in prediction. In observation, the NWPCCA is established in the preceding spring and lasts to summer through WES feedback associated with PMM. In prediction, the WES feedback is well predicted, including the persistence of the NWPCCA and equatorial Pacific warming from spring to summer. However, the predicted NWPCCA in summer is mainly forced by the enhanced convection over the subtropical central North Pacific due to the meridional SSTA gradient across the equator. The predicted westerly anomaly from the subtropical North Pacific arrives at the equator later than that in the observation, slowing down the warming rate over the equatorial CP in models.

Although ENSEMBLES successfully predicted those historical drought events, models still have difficulties in predicting the East Asian summer UTT cooling associated with North China summer drought events without well-established El Niño forcing. The East Asian UTT cooling is not only forced by the tropical forcings such as the Indian monsoon precipitation, but it is also greatly modulated by the mid–high-latitude atmosphere processes. One possible reason for this difficulty lies in the large chaos of the mid–high-latitude atmospheric processes, which are more evident in this type of events (Fig. 11c). Another possible reason lies in the weaker magnitude of Indian summer rainfall deficit in prediction compared with the observation, indicating a weaker tropical forcing for the Silk Road teleconnection (Figs. 6a,b and Figs. 11a,b). In MME, Walker circulation anomalies are not as strong as that in the observation due to a slower warming over the equatorial CP, and the associated Indian summer monsoon precipitation deficit is weaker than the observation. Besides the tropical forcing, extratropical SST over the Northern Hemisphere can also modulate the East Asian UTT by adjusting the displacement of the jet stream and setting up a quasi-stationary wave (Lau et al. 2004; Chattopadhyay et al. 2015). However, models show limiting ability in forecasting the SST anomalies over the middle and high latitudes of the North Pacific in the CP El Niño developing summer (Figs. 11a,b). An improvement on the prediction of SSTA warming rate over the central equatorial Pacific, the magnitude of the Indian

monsoon summer precipitation deficit, or the mid–high-latitude SSTA over the Northern Hemisphere may be helpful in a successful prediction of East Asian UTT cooling.

The reasonable hindcasts of North China summer drought in ENSEMBLES, particularly the prediction of precipitation deficit in drought years, are very encouraging for the development of climate services to aid preparation for future drought events. Most studies emphasized the predictive signal for the East Asian summer monsoon largely from EP El Niño, particularly the teleconnections in ENSO decaying summer. This study identified the predictive signal of PMM from subtropical central North Pacific SSTA one season before, which can be regarded as another important predictor of North China drought. We recognized the prediction uncertainty of North China drought due to model deficiency in predicting the midlatitude circulation anomalies. Further work is needed on improving the skill of circulation anomalies over the Asian continent by dynamical and statistical methods as Wang et al. (2017) suggested. We also examined the results predicting from 1 February by ENSEMBLES. There is no skill in predicting the North China summer drought when predicting by 4 months ahead, which may be related to the so-called spring predictability barrier of ENSO (Webster and Yang 1992). Investigations on the seasonal dependence of the prediction skill are needed in future studies.

Acknowledgments. This work was jointly supported by the National Natural Science Foundation of China under Grants 41661144009 and 41675076, the Key Research Program of the Chinese Academy of Sciences (ZDRW-ZS-2017-4), and the Program of International S&T Cooperation (2016YFE0102400). Peili Wu was supported by the U.K.–China Research and Innovation Partnership Fund through the Met Office Climate Science for Service Partnership (CSSP) China as part of the Newton Fund. The ENSEMBLES data used in this work were funded by the EU FP6 Integrated Project ENSEMBLES (Contract 505539), the support of which is gratefully acknowledged.

REFERENCES

Alexander, M., D. Vimont, P. Chang, and J. Scott, 2010: The impact of extratropical atmospheric variability on ENSO: Testing the seasonal footprinting mechanism using coupled model experiments. *J. Climate*, **23**, 2885–2901, https://doi.org/10.1175/2010JCLI3205.1.

Chattopadhyay, R., R. Phani, C. T. Sabeerali, A. R. Dhakate, K. D. Salunke, S. Mahapatra, A. Suryachandra Rao, and B. N. Goswami, 2015: Influence of extratropical sea-surface temperature on the Indian summer monsoon: An unexplored source of seasonal predictability. *Quart. J. Roy. Meteor. Soc.*, **141**, 2760–2775, https://doi.org/10.1002/qj.2562.

Chen, M., P. Xie, J. E. Janowiak, and P. A. Arkin, 2002: Global land precipitation: A 50-yr monthly analysis based on gauge observations. *J. Hydrometeor.*, **3**, 249–266, https://doi.org/10.1175/1525-7541(2002)003<0249:GLPAYM>2.0.CO;2.

Chiang, J., and D. J. Vimont, 2004: Analogous Pacific and Atlantic meridional modes of tropical atmosphere–ocean variability. *J. Climate*, **17**, 4143–4158, https://doi.org/10.1175/JCLI4953.1.

Chou, C., J. Tu, and J. Yu, 2003: Interannual variability of the western North Pacific summer monsoon: Differences between ENSO and non-ENSO years. *J. Climate*, **16**, 2275–2287, https://doi.org/10.1175/2761.1.

Ding, Q., and B. Wang, 2005: Circumglobal teleconnection in the Northern Hemisphere summer. *J. Climate*, **18**, 3483–3503, https://doi.org/10.1175/JCLI3473.1.

——, ——, J. Wallace, and G. Branstator, 2011: Tropical–extratropical teleconnections in boreal summer: Observed interannual variability. *J. Climate*, **24**, 1878–1896, https://doi.org/10.1175/2011JCLI3621.1.

Dutra, E., and Coauthors, 2014: Global meteorological drought—Part 2: Seasonal forecasts. *Hydrol. Earth Syst. Sci.*, **18**, 2669–2678, https://doi.org/10.5194/hess-18-2669-2014.

Enomoto, T., B. J. Hoskins, and Y. Matsuda, 2003: The formation mechanism of the Bonin high in August. *Quart. J. Roy. Meteor. Soc.*, **129**, 157–178, https://doi.org/10.1256/qj.01.211.

Gao, Y., H. Wang, and D. Chen, 2015: The capability of ENSEMBLES models in predicting the principal modes of pan-Asian monsoon precipitation. *J. Climate*, **28**, 8486–8510, https://doi.org/10.1175/JCLI-D-15-0010.1.

Hao, Z., A. AghaKouchak, N. Nakhjiri, and A. Farahmand, 2014: Global Integrated Drought Monitoring and Prediction System. *Sci. Data*, **1**, 140001, https://doi.org/10.1038/sdata.2014.1.

He, C., and T. Zhou, 2014: The two interannual variability modes of the western North Pacific subtropical high simulated by 28 CMIP5-AMIP models. *Climate Dyn.*, **43**, 2455–2469, https://doi.org/10.1007/s00382-014-2068-x.

Huang, R., and F. Sun, 1992: Impacts of the tropical western Pacific on the East Asian summer monsoon. *J. Meteor. Soc. Japan*, **70**, 243–256, https://doi.org/10.2151/jmsj1965.70.1B_243.

Kalnay, E., and Coauthors, 1996: The NCEP/NCAR 40-Year Reanalysis Project. *Bull. Amer. Meteor. Soc.*, **77**, 437–470, https://doi.org/10.1175/1520-0477(1996)077<0437:TNYRP>2.0.CO;2.

Kang, I. S., and Coauthors, 2002: Intercomparison of GCM simulated anomalies associated with the 1997/98 El Niño. *J. Climate*, **15**, 2791–2805, https://doi.org/10.1175/1520-0442(2002)015<2791:IOAGSA>2.0.CO;2.

Kim, H. M., P. J. Webster, J. A. Curry, and V. E. Toma, 2012: Asian summer monsoon prediction in ECMWF System 4 and NCEP CFSv2 retrospective seasonal forecasts. *Climate Dyn.*, **39**, 2975–2991, https://doi.org/10.1007/s00382-012-1470-5.

Kosaka, Y., and H. Nakamura, 2010: Mechanisms of meridional teleconnection observed between a summer monsoon system and a subtropical anticyclone. Part I: The Pacific–Japan pattern. *J. Climate*, **23**, 5085–5108, https://doi.org/10.1175/2010JCLI3413.1.

Lau, K.-M., J.-Y. Lee, K.-M. Kim, and I.-S. Kang, 2004: The North Pacific as a regulator of summertime climate over Eurasia and North America. *J. Climate*, **17**, 819–833, https://doi.org/10.1175/1520-0442(2004)017<0819:TNPAAR>2.0.CO;2.

Li, C., and Z. D. Lin, 2015: Predictability of the summer East Asian upper-tropospheric westerly jet in ENSEMBLES multi-model forecasts. *Adv. Atmos. Sci.*, **32**, 1669–1682, https://doi.org/10.1007/s00376-015-5057-z.

——, R. Lu, and B. Dong, 2012: Predictability of the western North Pacific summer climate demonstrated by the coupled models of ENSEMBLES. *Climate Dyn.*, **39**, 329–346, https://doi.org/10.1007/s00382-011-1274-z.

——, and Coauthors, 2016: Skillful seasonal prediction of Yangtze river valley summer rainfall. *Environ. Res. Lett.*, **11**, 094002, https://doi.org/10.1088/1748-9326/11/9/094002.

Luo, L., W. Tang, Z. Lin, and E. Wood, 2013: Evaluation of summer temperature and precipitation predictions from NCEP CFSv2 retrospective forecast over China. *Climate Dyn.*, **41**, 2213–2230, https://doi.org/10.1007/s00382-013-1927-1.

Ma, F., X. Yuan, and A. Ye, 2015: Seasonal drought predictability and forecast skill over China. *J. Geophys. Res.*, **120**, 8264–8275, https://doi.org/10.1002/2015JD023185.

Ma, Z., and C. Fu, 2006: Some evidence of drying trend over northern China from 1951 to 2004. *Chin. Sci. Bull.*, **51**, 2913–2925, https://doi.org/10.1007/s11434-006-2159-0.

McKee, T. B., N. J. Doesken, and J. Kleist, 1993: The relationship of drought frequency and duration to time scales. Preprints, *Eighth Conf. on Applied Climatology*, Anaheim, CA, Amer. Meteor. Soc., 179–184.

Mo, K., and B. Lyon, 2015: Global meteorological drought prediction using the North American Multi-Model Ensemble. *J. Hydrometeor.*, **16**, 1409–1424, https://doi.org/10.1175/JHM-D-14-0192.1.

Nitta, T., 1987: Convective activities in the tropical western Pacific and their impact on the Northern Hemisphere summer circulation. *J. Meteor. Soc. Japan*, **65**, 373–390, https://doi.org/10.2151/jmsj1965.65.3_373.

Rayner, N., D. E. Parker, E. B. Horton, C. K. Folland, L. V. Alexander, D. P. Rowell, E. C. Kent, and A. Kaplan, 2003: Global analyses of sea surface temperature, sea ice, and night marine air temperature since the late nineteenth century. *J. Geophys. Res.*, **108**, 4407, https://doi.org/10.1029/2002JD002670.

Thornthwaite, C. W., 1948: An approach toward a rational classification of climate. *Geogr. Rev.*, **38**, 55–94, https://doi.org/10.2307/210739.

Turco, M., A. Ceglar, C. Prodhomme, A. Soret, A. Toreti, and J. Doblas-Reyes Francisco, 2017: Summer drought predictability over Europe: Empirical versus dynamical forecasts. *Environ. Res. Lett.*, **12**, 084006, https://doi.org/10.1088/1748-9326/aa7859.

Vicente-Serrano, S. M., S. Beguería, and J. I. Lopez-Moreno, 2010: A multiscalar drought index sensitive to global warming: The standardized precipitation evapotranspiration index. *J. Climate*, **23**, 1696–1718, https://doi.org/10.1175/2009JCLI2909.1.

Vimont, D., D. Battisti, and A. Hirst, 2001: Footprinting: A seasonal connection between the tropics and mid-latitudes. *Geophys. Res. Lett.*, **28**, 3923–3926, https://doi.org/10.1029/2001GL013435.

——, ——, and ——, 2003a: The seasonal footprinting mechanism in the CSIRO general circulation models. *J. Climate*, **16**, 2653–2667, https://doi.org/10.1175/1520-0442(2003)016<2653:TSFMIT>2.0.CO;2.

——, J. Wallace, and D. Battisti, 2003b: The seasonal footprinting mechanism in the Pacific: Implications for ENSO. *J. Climate*, **16**, 2668–2675, https://doi.org/10.1175/1520-0442(2003)016<2668:TSFMIT>2.0.CO;2.

——, M. A. Alexander, and A. Fontaine, 2009: Midlatitude excitation of tropical variability in the Pacific: The role of thermodynamic coupling and seasonality. *J. Climate*, **22**, 518–534, https://doi.org/10.1175/2008JCLI2220.1.

Wang, B., and Coauthors, 2009: Advance and prospectus of seasonal prediction: Assessment of the APCC/CliPAS 14-model ensemble retrospective seasonal prediction (1980–2004). *Climate Dyn.*, **33**, 93–117, https://doi.org/ 10.1007/s00382-008-0460-0.

Wang, H., and S. He, 2015: The North China/northeastern Asia severe summer drought in 2014. *J. Climate*, **28**, 6667–6681, https://doi.org/10.1175/JCLI-D-15-0202.1.

Wang, S., X. Yuan, and Y. Li, 2017: Does a strong El Niño imply a higher predictability of extreme drought? *Sci. Rep.*, **7**, 40741, https://doi.org/10.1038/srep40741.

Webster, P. J., and S. Yang, 1992: Monsoon and ENSO: Selectively interactive systems. *Quart. J. Roy. Meteor. Soc.*, **118**, 877–926, https://doi.org/10.1002/qj.49711850705.

Weisheimer, A., and Coauthors, 2009: ENSEMBLES: A new multi-model ensemble for seasonal-to-annual predictions—Skill and progress beyond DEMETER in forecasting tropical Pacific SSTs. *Geophys. Res. Lett.*, **36**, L21711, https://doi.org/10.1029/2009GL040896.

Wen, N., Z. Liu, and L. Li, 2018: Direct ENSO impact on East Asian summer precipitation in the developing summer. *Climate Dyn.*, **4**, 1–17, https://doi.org/10.1007/s00382-018-4545-0.

Wu, J., and X. Gao, 2013: A gridded daily observation dataset over China region and comparison with the other datasets (in Chinese). *Chin. J. Geophys.*, **56**, 1102–1111.

Wu, R., Z. Hu, and B. Kirtman, 2003: Evolution of ENSO-related rainfall anomalies in East Asia. *J. Climate*, **16**, 3742–3758, https://doi.org/10.1175/1520-0442(2003)016<3742:EOERAI>2.0.CO;2.

Wu, S., L. Wu, Q. Liu, and S.-P. Xie, 2010: Development processes of the tropical Pacific meridional mode. *Adv. Atmos. Sci.*, **27**, 95–99, https://doi.org/10.1007/s00376-009-8067-x.

Yang, P., Z. Xiao, J. Yang, and H. Liu, 2013: Characteristics of clustering extreme drought events in China during 1961–2010. *Acta Meteor. Sin.*, **27**, 186–198, https://doi.org/10.1007/s13351-013-0204-x.

Yang, S., Z. Zhang, V. E. Kousky, R. W. Higgins, S.-H. Yoo, J. Liang, and Y. Fan, 2008: Simulations and seasonal prediction of the Asian summer monsoon in the NCEP Climate Forecast System. *J. Climate*, **21**, 3755–3775, https://doi.org/10.1175/2008JCLI1961.1.

Yeh, S. W., X. Wang, C. Wang, and B. Dewitte, 2015: On the relationship between the North Pacific climate variability and the central Pacific El Niño. *J. Climate*, **28**, 663–677, https://doi.org/10.1175/JCLI-D-14-00137.1.

Yu, J.-Y., Y. Zou, S. T. Kim, and T. Lee, 2012: The changing impact of El Niño on US winter temperatures. *Geophys. Res. Lett.*, **39**, L15702, https://doi.org/10.1029/2012GL052483.

Zhang, L., and T. Zhou, 2012: The interannual variability of summer upper-tropospheric temperature over East Asia. *J. Climate*, **25**, 6539–6553, https://doi.org/10.1175/JCLI-D-11-00583.1.

——, and ——, 2015: Drought over East Asia: A review. *J. Climate*, **28**, 3375–3399, https://doi.org/10.1175/JCLI-D-14-00259.1.

——, P. Wu, T. Zhou, and C. Xiao, 2018: ENSO transition from La Niña to El Niño drives prolonged spring–summer drought over North China. *J. Climate*, **31**, 3509–3523, https://doi.org/10.1175/JCLI-D-17-0440.1.

Zhou, T., D. Gong, J. Li, and B. Li, 2009: Detecting and understanding the multi-decadal variability of the East Asian summer monsoon—Recent progress and state of affairs. *Meteor. Z.*, **18**, 455–467, https://doi.org/10.1127/0941-2948/2009/0396.